NASA/TM—2019-220361

An Innovative Feedback Controls Design Approach for Aero Engines

George Kopasakis
Glenn Research Center, Cleveland, Ohio

Scott B. Norin
Vantage Partners, LLC, Brook Park, Ohio

November 2019

NASA STI Program . . . in Profile

Since its founding, NASA has been dedicated to the advancement of aeronautics and space science. The NASA Scientific and Technical Information (STI) Program plays a key part in helping NASA maintain this important role.

The NASA STI Program operates under the auspices of the Agency Chief Information Officer. It collects, organizes, provides for archiving, and disseminates NASA's STI. The NASA STI Program provides access to the NASA Technical Report Server—Registered (NTRS Reg) and NASA Technical Report Server—Public (NTRS) thus providing one of the largest collections of aeronautical and space science STI in the world. Results are published in both non-NASA channels and by NASA in the NASA STI Report Series, which includes the following report types:

- TECHNICAL PUBLICATION. Reports of completed research or a major significant phase of research that present the results of NASA programs and include extensive data or theoretical analysis. Includes compilations of significant scientific and technical data and information deemed to be of continuing reference value. NASA counter-part of peer-reviewed formal professional papers, but has less stringent limitations on manuscript length and extent of graphic presentations.

- TECHNICAL MEMORANDUM. Scientific and technical findings that are preliminary or of specialized interest, e.g., "quick-release" reports, working papers, and bibliographies that contain minimal annotation. Does not contain extensive analysis.

- CONTRACTOR REPORT. Scientific and technical findings by NASA-sponsored contractors and grantees.

- CONFERENCE PUBLICATION. Collected papers from scientific and technical conferences, symposia, seminars, or other meetings sponsored or co-sponsored by NASA.

- SPECIAL PUBLICATION. Scientific, technical, or historical information from NASA programs, projects, and missions, often concerned with subjects having substantial public interest.

- TECHNICAL TRANSLATION. English-language translations of foreign scientific and technical material pertinent to NASA's mission.

For more information about the NASA STI program, see the following:

- Access the NASA STI program home page at http://www.sti.nasa.gov

- E-mail your question to help@sti.nasa.gov

- Fax your question to the NASA STI Information Desk at 757-864-6500

- Telephone the NASA STI Information Desk at 757-864-9658

- Write to:
  NASA STI Program
  Mail Stop 148
  NASA Langley Research Center
  Hampton, VA 23681-2199

NASA/TM—2019-220361

An Innovative Feedback Controls Design Approach for Aero Engines

George Kopasakis
Glenn Research Center, Cleveland, Ohio

Scott B. Norin
Vantage Partners, LLC, Brook Park, Ohio

National Aeronautics and
Space Administration

Glenn Research Center
Cleveland, Ohio 44135

November 2019

Acknowledgments

The authors would like to thank the NASA Airspace Operations and Safety Program (AOSP)/ System-Wide Safety (SWS) Project/ Technologies for Airplane State Awareness (TASA)/SE-209 Simulator Fidelity for supporting this work. The authors would also like to acknowledge Mr. Jonathan S. Litt as the technical lead for this project and for his review of this paper and helpful comments.

Level of Review: This material has been technically reviewed by technical management.

Available from

NASA STI Program
Mail Stop 148
NASA Langley Research Center
Hampton, VA 23681-2199

National Technical Information Service
5285 Port Royal Road
Springfield, VA 22161
703-605-6000

This report is available in electronic form at http://www.sti.nasa.gov/ and http://ntrs.nasa.gov/

An Innovative Feedback Controls Design Approach for Aero Engines

George Kopasakis
National Aeronautics and Space Administration
Glenn Research Center
Cleveland, Ohio 44135

Scott B. Norin
Vantage Partners, LLC
Brook Park, Ohio 44142

Abstract

The paper describes a feedback controls design approach for a generic regional jet turbofan engine, which can be adapted to aero engines in general. To demonstrate this approach, linear models for control design are generated at different operating conditions from a full envelope nonlinear simulation created with the NASA Glenn Research Center-developed Toolbox for the Modeling and Analysis of Thermodynamic Systems. The primary objective is to design a single feedback controller that achieves good performance, without the need of developing scheduled control designs to cover the engine operating envelope. An additional objective is to progressively design more robust controllers that can perform under large variations in plant dynamics to also cover control for engine limits and potentially for some off nominal or even damaged conditions.

1.0 Introduction

The dynamics of aircraft engines vary substantially around the operating envelope, which is why engine controllers are typically gain scheduled. Engine feedback controllers are designed to control either the low spool speed (N1) or the Engine Pressure Ratio (EPR), by metering the fuel into the burner. Scheduled controllers are designed individually for each of the predetermined operating conditions, as well as for the different safety limits imposed on the engine for a given operating condition, which can become a laborious process. The objective here is to expedite the process by designing a single controller with globally acceptable performance that will cover the entire operating envelope, which potentially includes engine limits.

The Toolbox for the Modeling and Analysis of Thermodynamic Systems (T-MATS) (Ref. 1) is used here to model a generic regional jet (GRJ) turbofan engine. The T-MATS model was developed from engine cycle analysis performed using the Numerical Propulsion System Simulation (NPSS). The T-MATS GRJ turbofan engine model is linearized at different operating conditions to get corresponding linear models or Transfer Functions (TF) of the engine plant, which are used to design feedback controls.

The controller design is based on the loop shaping (LS) method described in Reference 2. In Reference 2 the approach was developed to design the controller and its bandwidth for a single plant TF based on the speed of its actuator. Here, however, the approach is used to design a feedback controller for a plant TF with approximately the average steady state proportional gain of the plant or with a plant step response that is deemed to be situated about half way between the individual responses (for both the rise time and for the steady state). Then this controller design is simulated for all the plant TFs selected to cover the engine operating conditions in order to evaluate how well this control design is able to maintain

desirable performance. Thus, the control bandwidth design carried out in Reference 2, which also safeguards the actuator (not to exceed its speed limit), may not be met in this design.

The control design itself is subdivided into three different control elements. First, a low frequency or a simplified control design structure is developed to be used as a baseline for comparisons with more complex control designs. An additional objective of this control design, referred to here as "the slow control design," is that it will be faster in terms of execution time (the required sampling frequency is lower) and is therefore more likely to be able to run in real time. Second, a fast control loop design is introduced that takes maximum advantage of the speed of the fuel actuator (Ref. 2). Finally, an adaptive gain control structure is employed based on the positive gradient control methodology described in Reference 3 and comparisons are performed. This adaptive control design is introduced here as an additional tool with the potential of embedding more robustness in the control with the ability to handle even more uncertainty in the plant dynamics.

The paper is organized as follows. First, engine plant models under different operating conditions are introduced in the form of TFs. This is followed by a description of the three control designs and results that demonstrate the effectiveness of those control approaches. Next, control system simulation results using the full envelope nonlinear T-MATS model are presented and compared with those obtained from the linear system models. Finally, concluding remarks are presented.

2.0 Linear GRJ Turbofan Engine Models

Table I shows the engine conditions for which linear models were developed using T-MATS. The plant TFs are *N1*(rpm)/$\dot{W}_F$(lb/s). As seen in this table, there are significant variations in plant dynamics, especially for the proportional gain (i.e., the proportional gain in a *normalized TF form* (Ref. 2) or the steady state gain), which varies over a range of approximately 1 to 10 times. The TFs for other nominal operating conditions are encompassed within the range of the TF gains shown in this table. The corresponding step responses of these TFs, which are labeled in order as Plant1 to Plant4, are shown in Figure 1. A mid-plant TF is constructed with a gain of 2,500 as mid-plant=(2,500/1,909)*Plant1, to be used for control design. The proportional gain of this plant is about half way between the extreme gains shown in the table.

3.0 Feedback Control Design for the GRJ Turbofan Engine

The LS control law designs described herein, for the GRJ Turbofan engine, primarily follow the approach described in Reference 2. The reader is encouraged to consult this reference for more detail, as the design methodology will not be repeated in this paper. The difference is that instead of using the actuator speed limit to design the controller and its bandwidth for a single plant TF (Ref. 2), the fuel actuator speed limit is used here to design the control system bandwidth based on one of the plant models. However, since the objective is to use the same controller design to accommodate large variations in plant dynamics, the designed control bandwidth will not necessarily be met for all the plant variations. The control design will be done in progressive steps, starting from the simplified or the slow LS feedback control design with a step response designed to meet the FAA requirement of 95 percent thrust response within 5 s (Ref. 4). This is followed by a fast loop control design that still meets the FAA requirement, but with better performance. Finally, the adaptive gain control design will be demonstrated.

3.1 A Slow Control Design

The slow LS feedback control design is intended to establish a baseline for comparison of control system performance for the subsequent control designs, as well as to allow fast execution for real time engine control applications because it doesn't require high frequency sampling. The LS control design here follows the same steps as those covered in Reference 2, whereby the desired open loop TF is selected

as G_d=3.3(s/0.33+1)/(s(s/1.0+1)) in order to have the desirable open loop shape, while the representative feedback control system meets the 5 s response requirement. The feedback response for this desired open loop TF is shown in Figure 2.

Aero engine fuel actuators are assumed to have a typical bandwidth of 6 Hz, and a corresponding simplified and damped TF with such a bandwidth would be G_a=1,369/(s^2+81.4s+1,369), which is also included as part of the plant. The Bode diagram of the desired open loop TF, G_d, is first plotted, and using the combined actuator and Mid-Plant TFs, the controller is designed to match the Bode plot of G_d. The method used here for this process is described in Appendix II of Reference 2, whereby the 3 dB separation in the respective gains is located and a pole or a zero is inserted appropriately at that frequency. The process is repeated in order for these gains to match well, at least up to the cross-over frequency. As seen in Figure 3, the last step (i.e., Bode plot of G_{c4} times Plant) matches well with the Bode plot of G_d up to the cross-over frequency of 10 rad/s, with some compromise in phase margin (PM) or system damping. If the desire is to preserve the PM of G_d, the responses would need to match at higher frequencies. However, this would require faster dynamics and a decrease in the integration step time for the simulation. This design process resulted in the following controller TF:

$$G_c=(3.3/2500)(s/0.33+1)(s/1.32+1)(s/8.6+1)/s(s/1.0+1)(s/3.2+1)$$

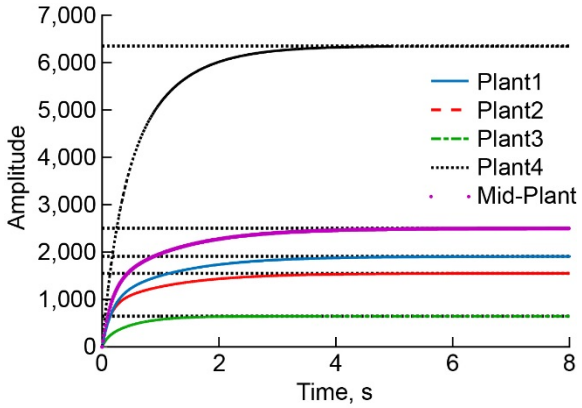

Figure 1.—Step response of the linearized engine plant models.

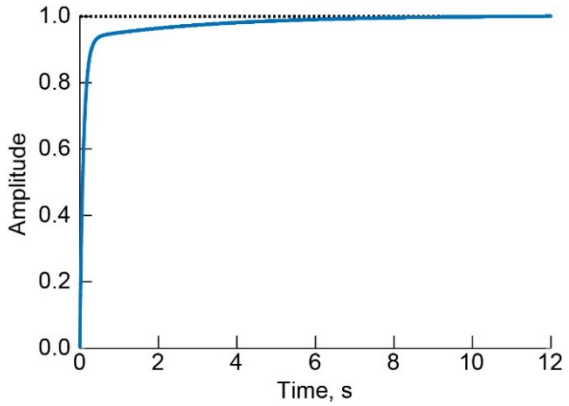

Figure 2.—Step response of the desired feedback system.

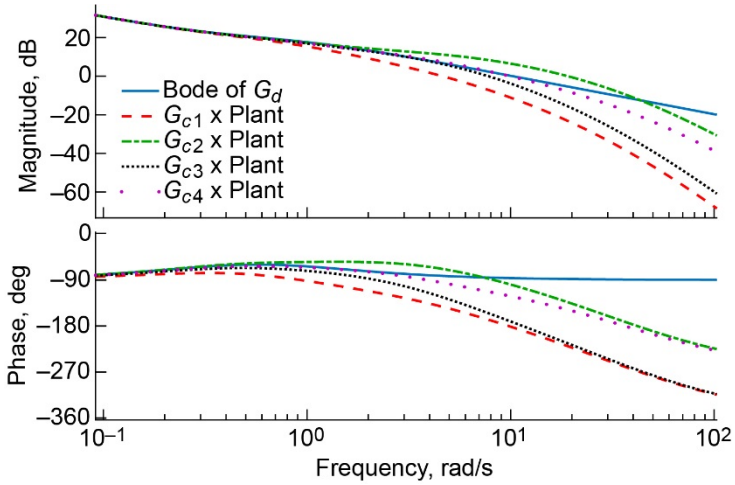

Figure 3.—Progressive matching of the plant times the controller with that of the desired open loop TFs.

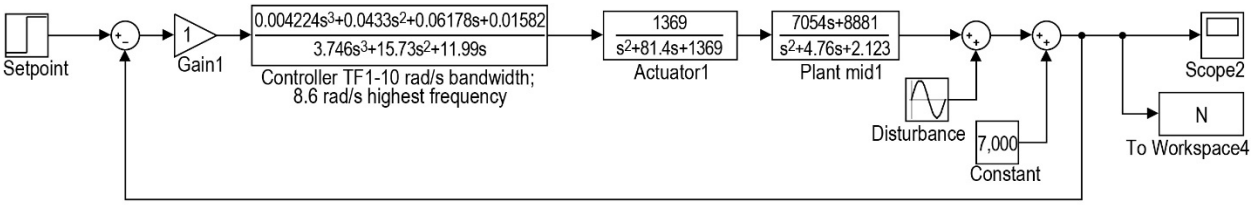

Figure 4.—Feedback controller design to meet 5 s response time.

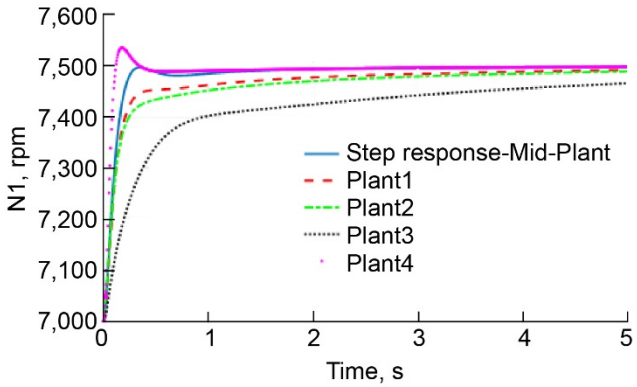

Figure 5.—Step responses of the control system with the different plant TFs.

The resulting feedback control system diagram with the evaluated controller TF is shown in the SIMULINK® model in Figure 4. For this control system setup, the speed N1 is set to be commanded starting from 7,000 rpm, with an optional speed disturbance applied, and with a proportional gain set to a value of 1, which signifies that the original plant proportional gain (i.e., the proportional gain of either a standardized or normalized TF, Ref. 2) remains as set. However, varying this gain allows testing the control system design with different proportional gains. Even though the disturbance in this control system model is speed, in a full T-MATS type engine simulation the disturbances would be quantities such as upstream total pressure and temperature or mass flowrate.

The step responses of this control system with all the plant TFs shown in Table I, including the mid-plant TF used for this control design, are shown in Figure 5 with no disturbance noise added. As shown in this figure, all the responses are stable with this LS control design. However, some of these responses fail to meet the 5 s settling time requirement. Note that these responses are linear (TF responses) and as such the step size chosen will not change the characteristics of the response.

The fastest pole/zero frequency in this control system design is that of the fuel actuator (37 rad/s). A common rule of thumb is to set the time step equal to the reciprocal of 5 to 10 times the highest frequency, which in this case is 1/5(37) or 0.0054 s. Practically however, the time step could be as large as 0.01 s and still maintain numerical stability or simulation accuracy. Since in this case the time step is dictated by the actuator, this design will have as fast execution as any possible control system design.

3.2 Fast Control Design

In this control system design the speed of the fuel actuator, which is normally approximately 6 Hz or 37 rad/s will be used to about its maximum ability to increase the bandwidth of the control system in order to improve the system performance. The LS approach in Reference 2 can also be used here to design a controller for the mid-plant discussed earlier, even though this single controller design may not

meet the maximum bandwidth desirable for the plant TFs. An alternative is to use a Model Following Control (MFC) design structure as covered in Appendix II of Reference 2, which will add more robustness to the control. In this section the former design approach will be used.

This LS control system design approach (Ref. 2) will be used here with the addition of a low pass filter inserted after the input command to control the response time to meet the 5 s requirement, while the control bandwidth can still be made much higher than this prescribed response time. This allows the control system to have the typical response time required, while significantly increasing its ability to reject disturbances. The SIMULINK® model for this control design is shown in Figure 6.

Since the LS control design described in Appendix II of Reference 2 is for a high bandwidth controller and since the plant model used for that design is not that much different than the mid-plant discussed here, for instance the gain of that plant was approximately 4,000 versus 2,500, the exact same control design is employed here as well. Restated here, the controller TF for this design is

$$G_c(s)=(9.102\times10^{6}s^{5}+7.987\times10^{8}s^{4}+1.728\times10^{10}s^{3}+8.844\times10^{10}s^{2}+1.609\times10^{11}s+9.665\times10^{10})/$$
$$(1.959\times10^{7}s^{5}+1.599\times10^{10}s^{4}+3.307\times10^{12}s^{3}+1.901\times10^{13}s^{2}+2.588\times10^{13}s)$$

Another purpose for using this controller design from Reference 2 instead of specifically designing a controller for the selected process, is to further demonstrate the robustness of the LS control design approach. The step responses of the control system with the different engine plant TFs discussed before, without any disturbance noise, are shown in Figure 7. The responses show that a single engine controller design as this provides for good performance that meets the 5 s response requirement. A high frequency padding pole on the order of 400 rad/s was added in the design described in Reference 2 to make the controller TF proper, but relatively good responses can still be obtained when this padding pole frequency is reduced to as little as 100 rad/s or slightly less. With this controller TF $G_c(s)$, the control system response for all the plants still meets the 5 s requirement, even when the plant proportional gain (Gain3 in Figure 6) varies in the range of 0.6 to 15 times. As such, this control design exhibits a relatively high degree of robustness.

These responses indicate that a single controller design should be able to cover the entire engine operating range without the need of gain scheduling control designs. Note, however, that by increasing the bandwidth of the controller beyond what is typically used, the control system may excite higher frequencies than that of the rotor dynamics or excite lower frequency gas dynamics. So a final check of this controller design should be against an engine model that includes volume dynamics (Refs. 5 and 6) or against real engine testbeds.

3.3 Adaptive Gain Control Design

Even though the engine plant variations under different vehicle operating conditions may be well covered with the plant TFs shown in Table I or with the control designs described in the previous sections, there could be additional unaccounted for conditions such as wear and tear, damage, or perhaps it may even be desirable to control engine limits with the same controller design. For a controller to be

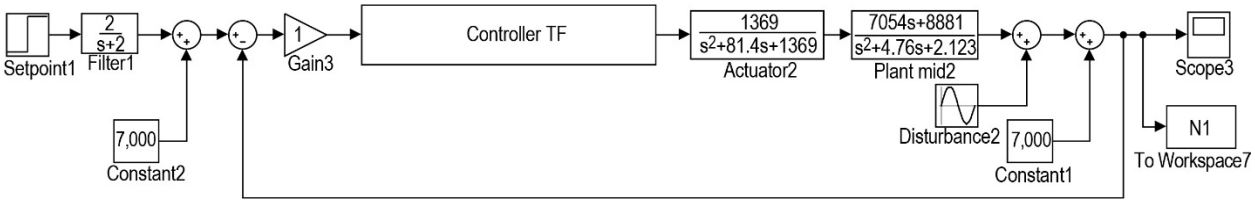

Figure 6.—Fast bandwidth controller with step command filter employed to meet required response time.

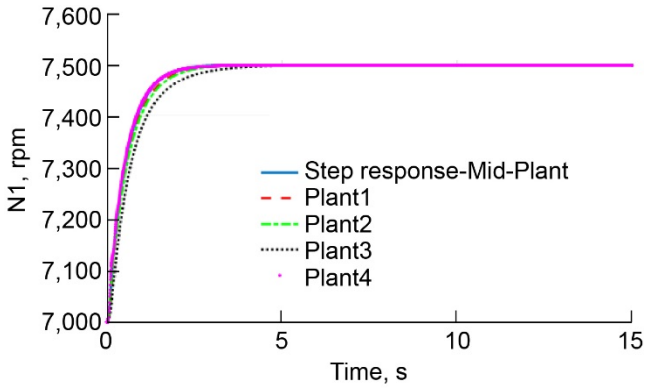

Figure 7.—Control system step response of the fast controller design in Figure 6 for all the engine plants in Table I.

TABLE I.—ENGINE OPERATING CONDITIONS AND TRANSFER FUNCTIONS

Operating C.	Mach no.	Altitude	dTamb	TF	Gain	Poles, rad/s	Zeros, rad/s
Cruise	0.8	35,000	0	$\frac{6616s+9969}{s^2+6.945s+5.222}$	1,909	–6.09, –0.86	–1.57
Mid-Cruise	0.5	25,000	0	$\frac{7203s+10500}{s^2+8.502s+6.769}$	1,550	–7.61, –0.89	–1.46
Takeoff	0	0	0	$\frac{2905s+1.664\times10^4}{s^2+15.03s+25.71}$	650	–13.04, –2.0	–5.73
Approach	0.3	0	0	$\frac{13720s+27120}{s^2+4.741s+4.271}$	6,350	–3.53, –1.21	–1.98

able to operate over such a wide range of operating conditions, it may be desirable for the controller design to exhibit even more robustness to variations in plant dynamics. Adaptive gain control methodologies are numerous in literature and an on-line search can produce a plethora of information on the subject. The objective here is to introduce a novel approach in this area with the potential to simplify the aero engine feedback control system design problem and possibly provide more design flexibility for applications where robust control system performance is of primary importance.

3.3.1 Positive Gradient Adaptive Gain Control Design

In this section an adaptive gain control methodology will be introduced that is based on the positive gradient or the performance seeking control methodology described in Reference 3. The performance control structure described in this reference was used to continuously adjust the control system setpoints in order to drive the system to the operating point that maximizes a performance objective. This was done by driving the process in the positive gradient direction of a performance function with respect to the control inputs. Mathematically, this is positive gradient control of the performance objective, f, with respect to the control input, u, (i.e., $\partial f/\partial u$).

For engine control, the MFC structure (Ref. 2) and the positive gradient control structure (Ref. 3) will be utilized to adapt the controller gain in an effort to handle plant uncertainties via a performance objective that minimizes the error between the control system and a reference model. In the process of formulating the performance objective, it is desirable for an error value of zero to produce a maximum performance value, and as such the performance function chosen here is as follows: $f = (X_{ref} - R)^2 - (X_C - R)^2$, where X_{ref}, X_C, and R are the reference model output state, the control output state, and the setpoint, respectively. Notice

that advantageously this function is quadratic and convex with a global maximum, which describes a three-dimensional surface resembling a hill, whose maximum value is 0 at the point (X_{ref}, X_C) = (R, R). It may also be noticed that by squaring the terms in this function, the directional information that is necessary for the gradient computation is lost. Thus, this performance function is modified as follows in order to restore this information.

$$f = \left[-\left(X_{ref} - R\right)^2 - (X_C - R)^2\right] sign(X_{ref} - X_C) \tag{1}$$

With this modification however, the performance surface is changed to the original surface adjoined by its mirror image (upside down hill) at this extremum. Nevertheless, on either surface the sign of ∂u changes correspondingly with the sign of ∂f so that the positive gradient of $\partial f/\partial u$ is maintained at all times, and positive gradient trajectories operating on either surface are mirror images of each other. This also means that looking only at one of the surfaces is sufficient to see the evolution of the state trajectory, while the actual state trajectory near the extremum point may be jumping from one surface to the other.

The evaluation of the gradient, $\partial f/\partial u$, is done using a derivative approximation with a first order low pass filter used for causality (Ref. 3). Thus, the gradient approximation will not necessarily be normal to the surface elevation contours (Ref. 3), but nevertheless the state trajectory will still follow either an ascending or a descending path progressively advancing towards the extremum.

When adapting the controller gain, it would be expected that in the presence of noise, the positive gradient adaptation will continue to increase the gain in order to suppress noise. That is because increasing the controller gain increases the open loop TF gain or the control bandwidth, which increases attenuation of disturbances and maximizes the performance function in Equation (1). This can become problematic however, if at some point in the process the Phase margin (PM) or the Gain Margin (GM) of the feedback control system is depleted. One way to minimize the possibility of this happening is to turn off the adaptation when the reference model output and the control system output match within a certain value say, a noise tolerance as

$$\left|(X_{ref} - X_C)/X_{ref}\right| \leq N_t \tag{2}$$

where N_t is the approximate noise to signal ratio of the noise tolerance. If the control setpoint is moved starting from the value of 0 to 1, Equation (2) would be expected to enable adaptation as the value of X_{ref} in the denominator will also be small, while at steady state this relation will turn the adaptation off when the resulting noise amplitude from the control system is less than N_t. This could be an area where different functions for noise tolerance may be more suitable depending on the situation.

The adaptation feedback process is shown in the SIMULINK® diagram of Figure 8. The plant with the feedback controller TF design described in Appendix II of Reference 2 is also used here for the adaptive controller design. The reference model shown in Figure 8 is chosen to be the feedback TF of the desired open loop TF design, G_d (**G_d=15(s/1.5+1)/s(s/3.7+1)**), described in Reference 2. The reason for this is to make the bandwidth of the reference model the same as that of the inner loop control system, with as good performance. The mechanism for the adaptive gain portion is added to the *GainAdaptation* block shown in Figure 8. One of the inputs shown to the adaptation block comes from the output of the controller. Because what really matters here is the actuation action to the process rather than the controller output, this control input to the adaptation block is passed through the same actuator TF. This is done here, since in a physical implementation it is easier to directly access the digital signal. In addition, because a coupling oscillation in the adaptation loop is produced for the control input, the control signal here is further filtered by a first order filter of 10 rad/s in order to suppress high frequency oscillations.

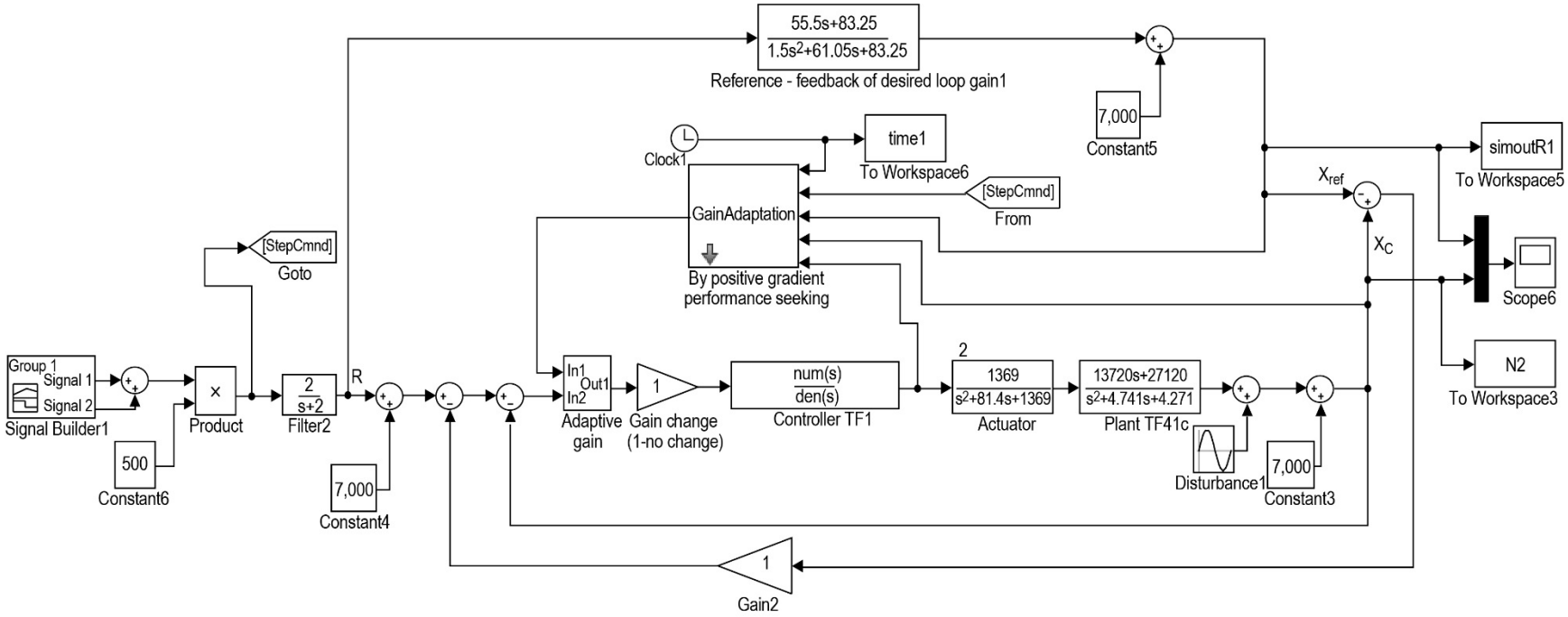

Figure 8.—Model Reference Positive Gradient Adaptive Control Design structure.

TABLE II.—ADAPTATION PARAMETERS

Parameter	Value
deadTime	0.001
MaxGain	100
MinGain	0.05
Omega	10
GradLimit+/-	1,000,000
IntegGain	0.005
NoiseThresh	0.2

The parameters that are used to tune this adaptation mechanism are constructed as a MASK in the GainAdaptation SIMULINK® block shown in Figure 8, and are listed in Table II. The *deadTime* parameter is used to allow the controller to start and initialize, before adaptation is enabled. The *MaxGain* and *MinGain* parameters set the range within which the adaptation gain is allowed to vary, and for the values listed in the table it permits a gain adaptation range from about 0.05 times to 100 times the original designed controller gain. The parameter *Omega* is used for the filter in the gradient derivative approximation Reference 3. The parameter *GradLimit+/-* is used to limit the output of the approximate gradient, $\partial f/\partial u$, to avoid getting excessively large or infinite values. The output of this gradient value is fed into an integrator Reference 3, and the parameter *IntegGain* is the gain of this integrator. This integrator gain is tuned to allow for fast adaptation in this case, but not so fast that the initial response to setpoint changes will end up being oscillatory. The parameter *NoiseThresh* is the noise threshold for which the adaptation is disabled when Equation (2) is satisfied. Even though the value shown in the table worked well for initial testing of the control system when the setpoint is varied around the values of +/- 1, this value had to be changed significantly for the N1 setpoint, as will be discussed later. All the parameters displayed in Table II are found to have low sensitivity, except perhaps for the parameter *NoiseThresh*.

3.3.2 Positive Gradient Adaptive Gain Method Results

An important aspect of the method described in Appendix II in Reference 2, which is also used here, is that the controller is designed so that the resulting open loop TF, including the padding pole, well matches both the gain and phase of the desired open loop gain, at least up to the cross-over frequency. This is done so that there is not a significant compromise to the PM, while the GM is still adequate. This makes the adaptive controller more robust. This is shown in Figure 9, where the PM at the cross-over frequency of about 37 rad/s is about 85°. With such a controller design, the open loop gains of all the plant TFs listed in Table I have relatively large PM of at least 75° despite their different cross-over frequencies, as shown in Figure 10.

Figure 11(a), shows an example control system response to set-point changes with the plant proportional gain of 0.01 **times** its original value and with 40 percent disturbance added at a frequency of 3 rad/s (for the same Mid-Plant). Figure 11(b) shows corresponding changes to the adaptive gain during the control process. Figure 12 shows the ascent of the state trajectory towards the extremum point on the performance surface for a typical run, while Figure 13 and Figure 14 show an ascent through performance elevation contours, with and without disturbance noise. As is evident from these figures and as described in Reference 3, the trajectory moves in an approximate positive gradient direction, until ascent in a particular direction ceases. At that point, a new ascent direction is established towards the maximum, and the process repeats. Simulations (not shown here) with 100 **times** the original plant gain show about the same results. Compared to the MFC structure described in Reference 2, this adaptive control design displays more robustness.

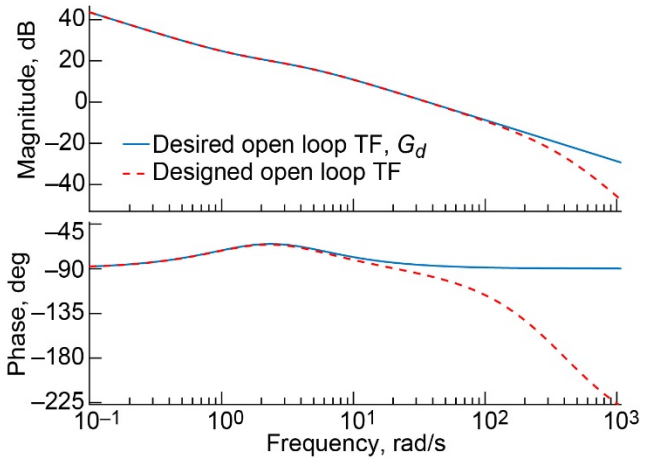

Figure 9.—Shows good matching of the open loop TF for this controller design to that of the desired TF.

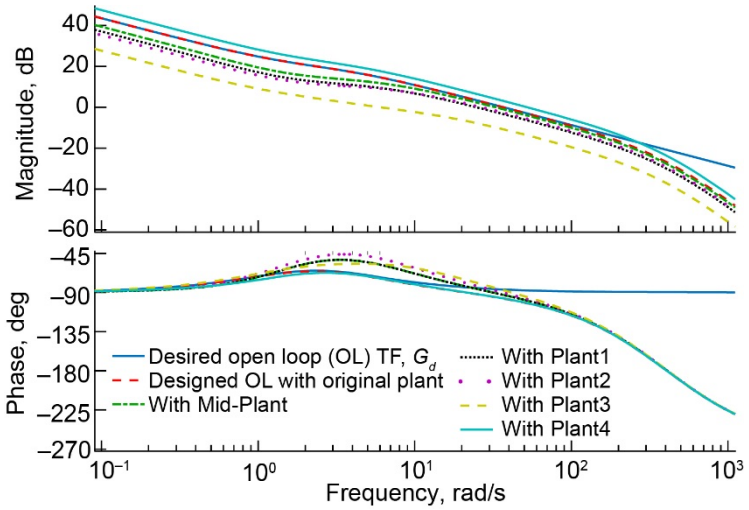

Figure 10.—Shows good matching of the open loop TF for this controller design to that of the desired TF with high PM.

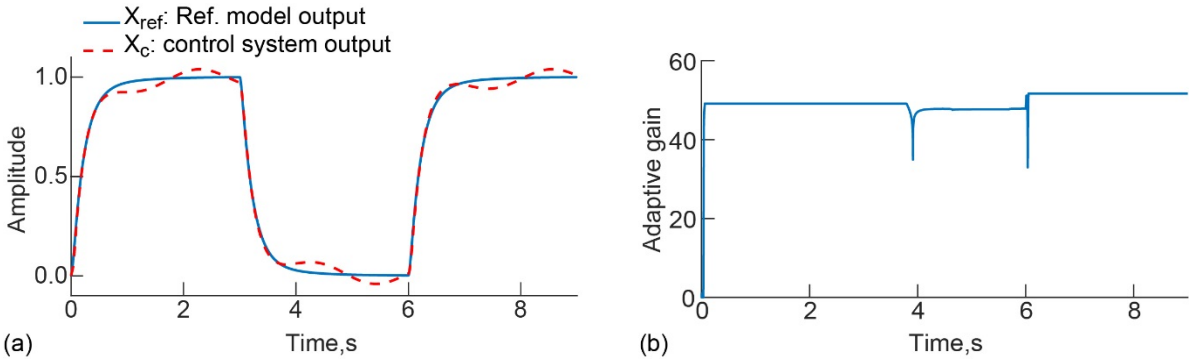

Figure 11.—Adaptive controller responses with a proportional gain of 0.01 times its original value and 40 percent noise, (a) Control system step response, (b) Adaptive gain response.

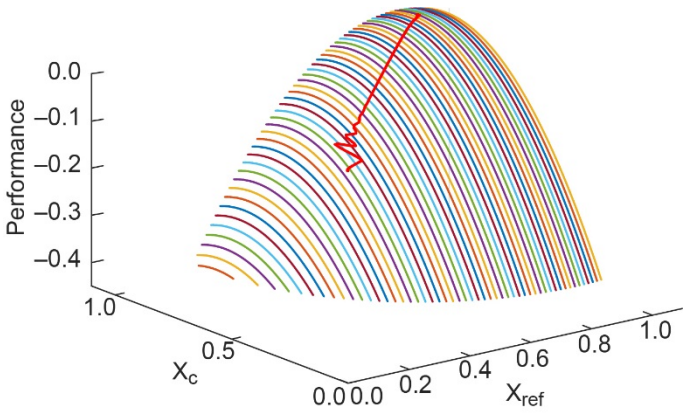

Figure 12.—A slice of the performance surface and the output state trajectory ascending to the top of the surface to the maximum performance point.

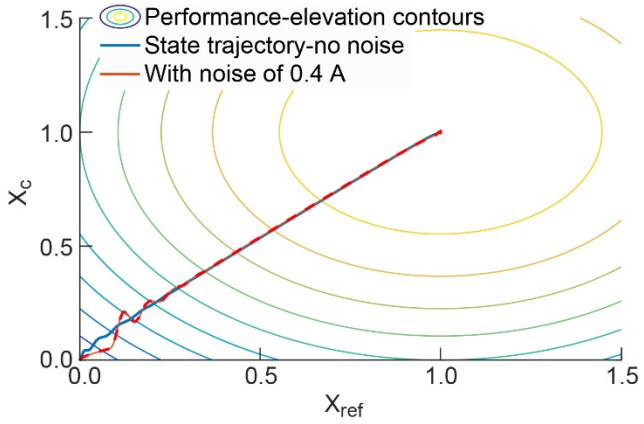

Figure 13.—Performance surface elevation contours and the output state trajectory ascending through the elevation contours, with and without noise in the system.

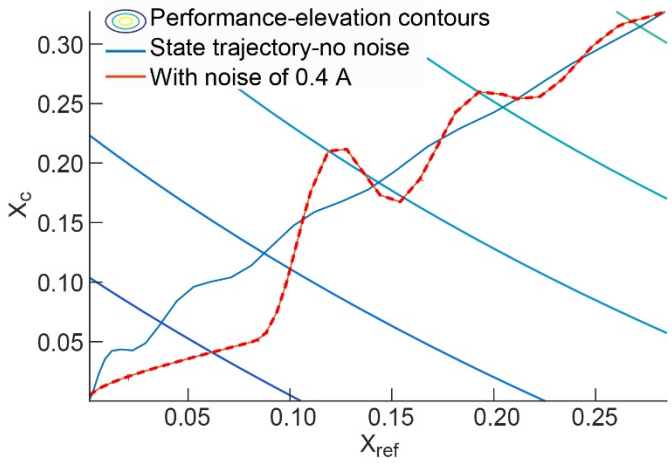

Figure 14.—Zoom in of Figure 12 to show that when ascent in a certain direction stops, a new ascent direction is established by the positive gradient and the trajectory continues to climb towards the extremum.

The response of the reference model in Figure 8 (i.e., the feedback TF of the desired open loop gain), has a damped response that meets the 5 s requirement. The adaptive control system tracks the output of the reference model and any variations manifest as a setpoint change to the inner control loop.

The different plants in Table I are simulated in this control system, and they all track the reference model without any discernable differences in their responses. Varying the plant dynamics by varying the normalized proportional or steady state gain of the plant has been simulated in the range of 100 **times** to 0.03 **times** and still all the control system responses track very well. This is shown in Figure 15 and Figure 16, respectively, with a disturbance noise level of 50 rpm applied for both cases at a frequency of 3 rad/s. For a plant gain variation less than 0.03 **times**, the original plant gain the adaptive controller starts having problems tracking the reference model. For this adaptive controller, all the tuning parameters shown in Table II remain the same, except for the *NoiseThresh* parameter, which is tuned to a value of 0.003. This value is approximately *NoiseThresh*/NA, where NA is the maximum noise amplitude in this simulation and *NoiseThresh* is the value from Table II.

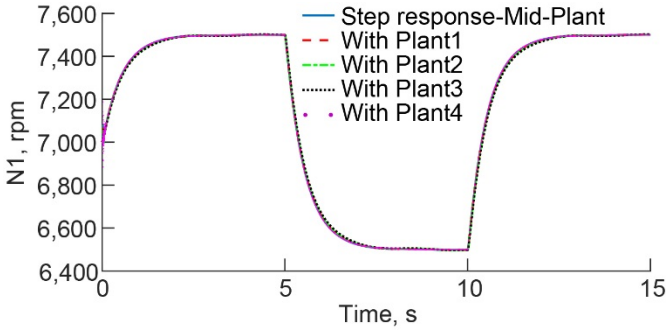

Figure 15.—Adaptive control system step response for all the engine plants in Table I, and with a plant proportional gain of 100 times the original gain.

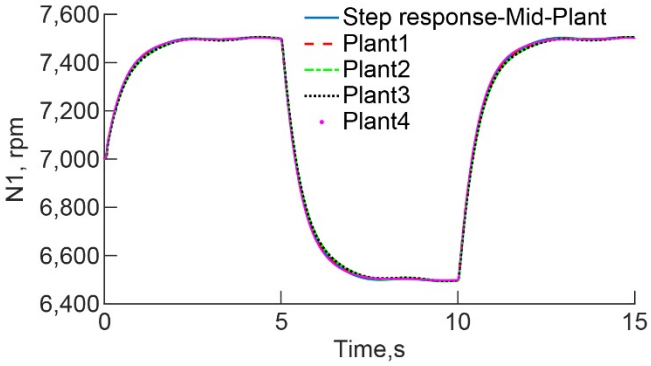

Figure 16.—Adaptive control system step response for all the engine plants in Table I, and with a plant proportional gain of 0.03 times the original gain.

4.0 T-MATS LS Controller Simulations

The LS controller designs described in the previous section were integrated into the nonlinear GRJ turbofan engine model developed in T-MATS, and simulations were carried out to validate the controller designs. First, relatively small throttle step commands that generated N1 step commands of 100 to 200 rpm were used to check the control system responses for the corresponding linear operating conditions described in the previous section, without engaging the limiters. Before the step commands were introduced, the simulation was allowed to run for a few seconds in order for the responses to arrive at a steady state or an equilibrium condition.

Unlike the simulations carried out in the previous section (500 rpm N1 step commands starting from 7,000 rpm), in the T-MATS simulations the starting rpm is different for each operating condition, while the size of the N1 commands are also different (i.e., the throttle position delta doesn't linearly correspond to N1 delta). For these reasons, the step responses here are normalized and plotted in order to compare them with each other and to also compare them with the responses shown in the previous section. Figure 17 show the normalized step responses of the T-MATS engine simulation with the slow feedback controller TF shown in Figure 4. One extra operating condition was included here for Taxi that turns out to have a TF proportional gain of 7,775, which is outside the range of the TF gains displayed in Table I. This extra condition is used to demonstrate that additional operating conditions can be included for these studies as desired or required. Comparing the T-MATS responses in Figure 17 with that of the linear control system responses in Figure 5, it can be seen that corresponding responses are similar, except for the undershoot/overshoot responses displayed here for the approach condition, which apparently is part of the nonlinear behavior of the engine model for this flight condition. Like those shown in Figure 5, not all the responses in Figure 17 meet the 5 s requirement. However, with the design and implementation of variable bleed valve (VBV) schedule (a Variable Guide Vane (VGV) schedule (Refs. 5 and 6) was already employed in this design), all the responses in T-MATS (not shown here) using the slow controller design do meet the 5 s requirement. The VBV or the VGV designs will not be covered here, as this goes beyond the objective of this paper. Even though the slow controller design with the addition of a VBV meets the FAA response time requirement, disturbance rejection or robustness will not be as good as with a faster controller design.

Similarly, the T-MATS engine responses for the faster controller design TF in Figure 6, are shown in Figure 18, which are comparable to the responses shown in Figure 7. In this case, all control system responses for the different operating conditions meet the desired or required response time of 5 s, without using the VBV schedule in these simulations.

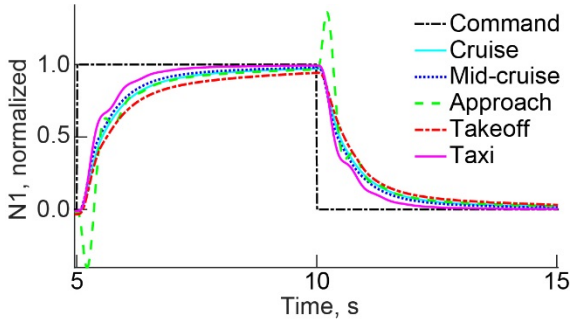

Figure 17.—Step responses of the nonlinear engine model at different operating conditions with the slow LS feedback controller design shown in Figure 4.

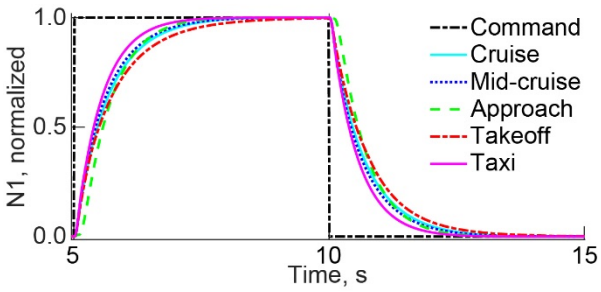

Figure 18.—Step responses of the nonlinear engine model at different operating conditions with the faster LS feedback controller design shown in Figure 6.

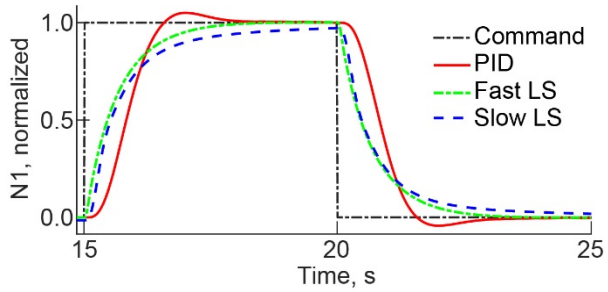

Figure 19.—Step responses of the nonlinear engine simulation at cruise for PID control designed for cruise compared with the fast and slow LS controllers of the previous design.

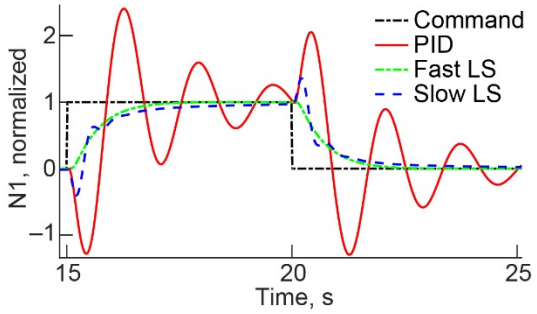

Figure 20.—Step responses of the nonlinear engine model at approach for PID control designed for cruise compared with the fast and slow LS controllers of the previous design.

For Aero engines, PID (Proportional Integral Derivative) control designs must be scheduled, in contrast to this LS control design, which is not. However, some perspective can be given here to show how a typical PID design is expected to respond for other flight conditions. Figure 19 and Figure 20 respectively, show step response comparisons of the slow and the fast control system designs discussed above against that of a PID control system designed for the cruise condition and run at cruise, and that of the same PID design run at the approach condition. As seen in Figure 20 the PID control system designed for cruise and run at the approach condition would be nearly unstable, while the same fast controller design for instance, is impervious to the condition change. There were other conditions for which this PID control system design was completely unstable.

Simulations were also run with T-MATS to show additional engine responses for various flight conditions. One of these simulated conditions is shown in Figure 21 for a throttle control action that ramps the engine speed, starting at 95 s, from near idle at sea level to 100 percent power in 5 s. Then the speed, N1, is slowly increasing during the next 30 s due to increasing Mach number, simulating a take-off, climb and leveling-off at 2,500 ft. The figure also shows the thrust response during this flight, the Stall Margin (SM) for the High Pressure Compressor (HPC) and the fan, and the Inter Turbine Temperature (ITT)—the gas temperature between the High Pressure Turbine and Low Pressure Turbine. As seen in Figure 21, the SM for the fan decreases during the acceleration portion of the flight envelope, while the HPC SM initially dips and then increases. The HPC SM is increasing during this transient because the bleed schedule kicks in at this time. The fan SM transient approaches nearly zero during the fast part of the transient. This is because the engine performance maps are not necessarily optimized, with a fan SM or a fan R-line that is situated closer to the stall line than what would normally be the case. The ITT is also significantly higher than what normally will be experienced. The reason for this is that the combustor stoichiometry is not simulated in this model. Thus, as significant air is diverted through the VBV, the combustor is burning rich and without taking into account its stoichiometry, the temperature increases significantly. Note that the objective here is not to exactly simulate an existing engine's performance, but rather to demonstrate an improved engine controls design methodology. As such, the important thing here is to observe control system responses and the trends rather than the actual numbers.

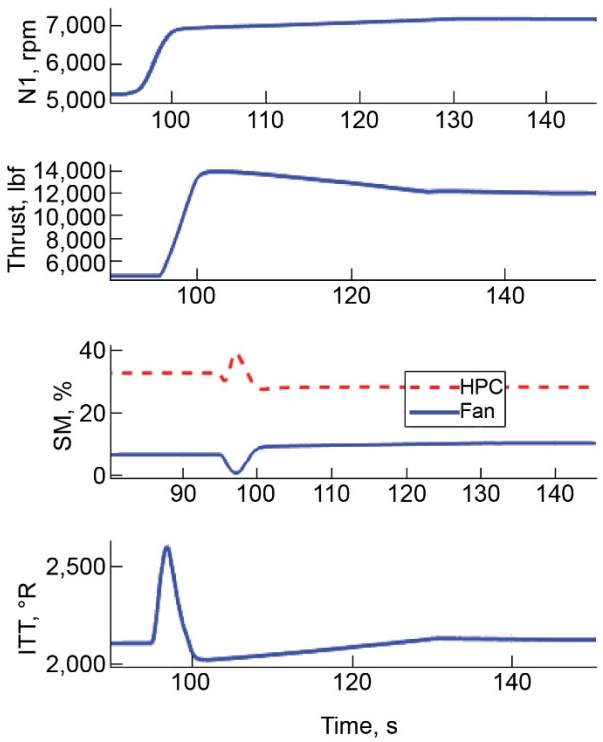

Figure 21.—Engine simulation responses to throttle action at 95 s and engine accelerating from near idle to about 100 percent speed. Then at 100 s a ramp is applied for the next 30 s—simulating sea-level take-off and leveling at 2,500 ft.

Next, the engine limits were tied back to the model to see how the same fast LS control design will be able to accommodate the limits for cases where the limits are engaged. The standard controller implementation in the T-MATS engine model uses a so-called *free integrator* at the output of the control structure (Ref. 7) with a scheduled gain. To implement the control design for the limiters, the same LS controller TF utilized before for N1 is also employed here for the limiters without the free integrator, whereby the selected error from the *Min-Max* logic is directly fed to the controller TF. Because the plant steady state proportional gains for the respective limiters vary significantly more than the gains shown in Table I (e.g., vary from 0.001 to 200 and in one case there is even a sign change with a gain of –5,000), the control system responses for the limiters were first tested and their respective gains were adjusted so that their responses approximated that of the fast LS controller shown in Figure 18 or Figure 19. So by employing the same controller TF as that of the fast controller for instance, only a gain value was set for each limiter.

The engine limiters were tested using step commands. Figure 22 shows the N2 limiter responses for different operating conditions, which were also found to be typical responses for the rest of the limiters. Due to the damped control system responses using the fast LS controller (see Figure 18), and perhaps due to the addition of VBV schedules, the engine limits are more difficult to engage with this control design.

For the adaptive controller, the T-MATS implementation is shown in Figure 23. Because several processes are simultaneously taking place in T-MATS, especially for larger step commands where the VGV and VBV are changing, it was found that some tuning or adjustments were necessary to implement the adaptive controller with the nonlinear engine simulation. Gain adaptation needed to be slowed down; a low pass filter was used for this purpose inside the *GainAdaptation* block. At the same time, it was found that the adaptation of the outer control loop needed to be sped up, and for that, the gain of the outer loop was increased from 1 to 3.

Figure 24 shows a step response of the engine speed due to a relatively sharp throttle deceleration/acceleration command at sea-level. The adaptive controller closely follows the response of the reference model. Figure 25 shows the fuel flow and engine gas temperature (ITT) during this transient. Because the adaptive controller closely follows the schedule command and closely hugs the reference model (see Figure 24), besides temperature, which is not well tuned in terms of performance, it is even more difficult to engage the limits with this controller, even compared to the fast controller design described earlier.

The adaptive as well as the fast controller discussed previously, have fast responses, significantly faster than that indicated by their overall response time, which is slowed down by filtering the input command. As such, these controllers also have better disturbance rejection capability (see Ref. 2).

Implementing the limits with the adaptive controller is more involved as the adaptive control structure needs to be changed as follows. The reference model shown in Figure 23 needs to be duplicated separately for each limiter while the respective limit values need to be used as the command input to the reference model; the “N1_int” (initial condition) needs to be set to zero after the initial startup transient; limit flags need to be set with the *Min-Max* logic to switch in the right command and sensed values for the controller to replace the “N1_sch” and “N1_sens” while the N1_sens value is also fed directly to the second summation block – ahead of the command filter; approximate gains for the limits, as used for the fast controller, may also need to be used for the “gain_change” block in Figure 23—this has not be done here. The gain approximation for the limits will likely need to be within an order of magnitude of the steady state value of the respective plant TF, as the adaptation mechanism will make necessary adjustments.

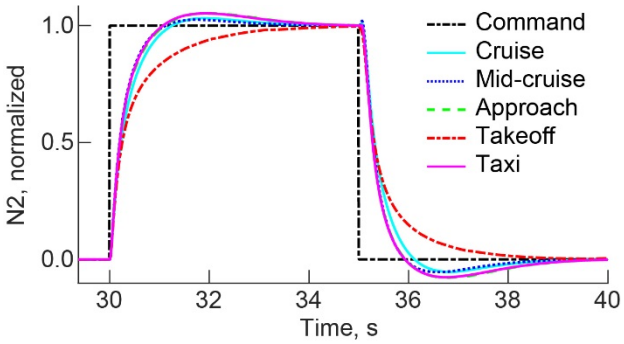

Figure 22.—Step responses of the engine N2 limit at different operating conditions for the fast LS controller.

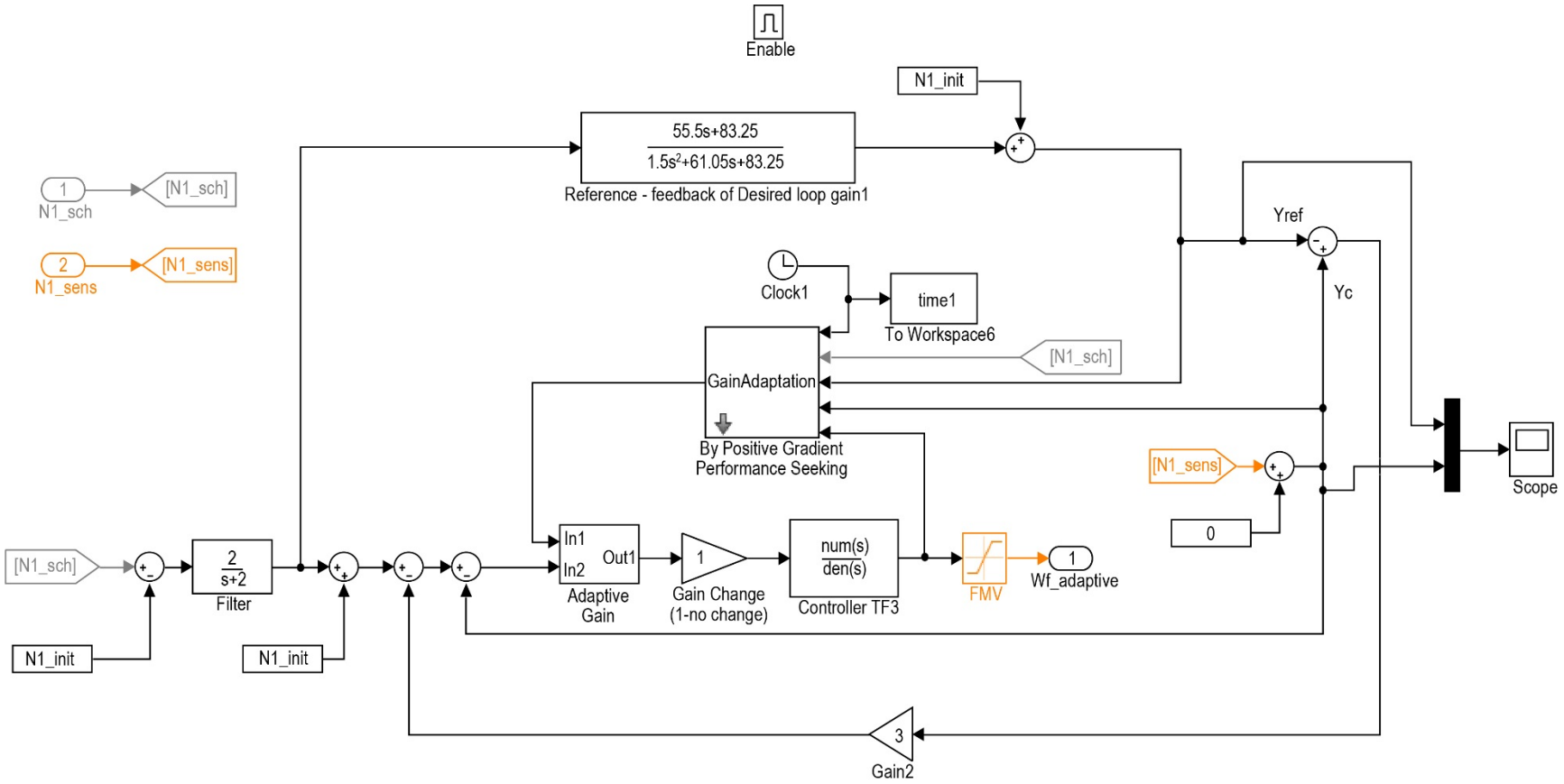

Figure 23.—T-MATS implementation of the model reference positive gradient adaptive control design.

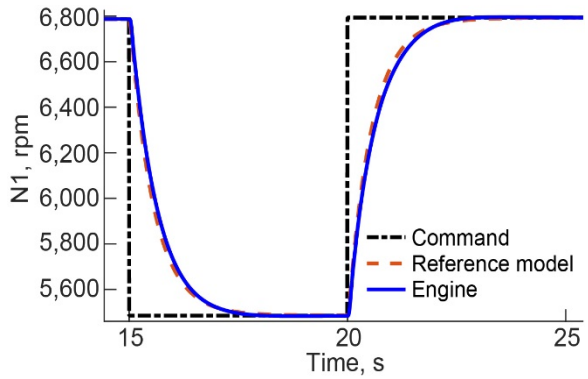

Figure 24.—Engine step response with the adaptive controller.

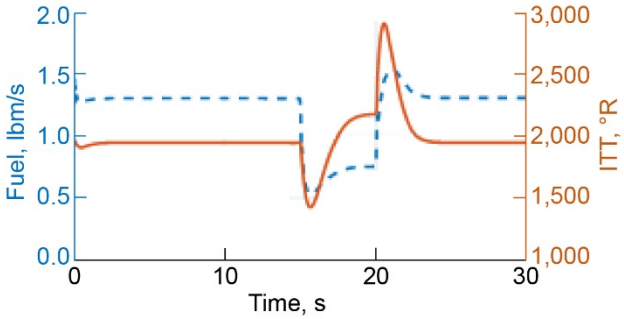

Figure 25.—Fuel and engine gas temperature during throttle step command.

5.0 Discussion and Conclusion

The paper demonstrated aero engine control designs based on the loop shaping (LS) technique published previously. The bandwidth of the control system in these designs can significantly differ from that of the LS methodology where the control bandwidth design is based on the actuator speed limit. This is because the same controller is used for large variations in plant dynamics in order to avoid the laborious exercise of designing engine control schedules. Normally, the control bandwidth design in the LS control methodology also safeguards against the process exceeding its speed limitations. In this case however, an actuator speed limiter should provide adequate safeguard in case the actuator speed limit is exceeded. The control designs in this paper start with the so-called slow LS controller and progress to a faster controller, and finally an adaptive control design. This evolution in the control designs covered in the paper is for the purpose of demonstrating a single controller design that covers all the operating modes of the engine as well as its safety limits, while it maintains some robustness. The control designs illustrated here using a turbofan engine simulation achieve these objectives, which demonstrates the potential to simplify and expedite aero engine controls designs in general by potentially eliminating the design of engine control schedules. The so-called slow control design was able to achieve the desirable engine response for all the engine operating conditions, but with the aid of a Variable Bleed Valve (VBV) schedule. The so called fast controller design described in the paper was shown to be able to cover the engine operating envelope also with a single controller design, with or without the VBV schedule. The same controller design was able to also handle the engine limits, but with proportional gain adjustments. The adaptive design achieves the same objectives as the fast controller, but with the additional possibility of adapting to engine changes such as engine health deterioration or even possibly damage. The implementation of the limits using the adaptive controller design is more involved and this part was not demonstrated in the paper.

References

1. Chapman, J. W.; Lavelle, T. M.; May, R. D.; Litt, J. S.; Guo, T. H.; “Propulsion System Simulation Using the Toolbox for the Modeling and Analysis of Thermodynamic Systems (T-MATS),” NASA/TM—2014-218410, Nov. 2014.
2. Kopasakis, G.; “Methodologies for Root Locus and Loop Shaping Control Design with Comparisons,” NASA/TM—2017-219721, Dec. 2017.

3. Kopasakis, G.; “Adaptive Performance Seeking Control using Fuzzy Model Reference Learning Control and Positive Gradient Control,” AIAA, 33rd JPC & Exhibit, Seattle WA, July 6-9, 1997, NASA TM-107455
4. Federal Aviation Administration, publication “14 CFR 33.73 - Power or thrust response.”
5. Connolly, J. W.; Kopasakis, G.; Carlson, J. R.; Woolwine, K.; “Nonlinear Dynamic Modeling of a Supersonic Commercial Transport Turbo-Machinery Propulsion System for Aero-Propulso-Servo-Elasticity Research,” 51st AIAA/SAE/ASEE Joint Propulsion Conference, July 27-29, 2015, Orlando, FL, AIAA 2015-4031.
6. Kopasakis, G.; Connolly, J. W.; Seidel, J. A.; Christhilf, D. M.; “Propulsion System Dynamic Modeling of the NASA Supersonic Concept Vehicle for Aero-Propulso-Servo-Elasticity,” 50th AIAA/ASME/SAE/ASEE Joint Propulsion Conference, July 28-30, 2014, Cleveland, OH, AIAA 2014-3684.
7. DeCastro, J. A.; Litt, J. S.; Frederick, D. K.; “A Modular Aero-Propulsion System Simulation of a Large Commercial Aircraft Engine,” AIAA-2008-4579, 44th AIAA/ASME/SAE/ASEE Joint Propulsion Conference & Exhibit, Hartford, CT, July 21-23, 2008.